JOURNAL OF GUIDANCE, CONTROL, AND DYNAMICS
Vol. 34, No. 3, May–June 2011

Engineering Notes

Orbit Determination with Improved Covariance Fidelity, Including Sensor Measurement Biases

Michael E. Hough*
Raytheon Company, Inc., Woburn, Massachusetts 01801

DOI: 10.2514/1.53053

I. Introduction

ORBIT determination algorithms based on the minimum variance (or Kalman) filter provide unbiased position and velocity estimates when sensor measurements contain only random errors. The Kalman filter covariance matrix is usually consistent with the bias-free estimation error statistics, indicating good covariance fidelity, when random error statistics are accurately characterized. However, sensor measurements often contain unmodeled static and dynamic measurement biases, or low-frequency systematic errors, that cause biases in the position and velocity estimates. In this situation, the Kalman filter covariance usually underestimates the error statistics, indicating poor covariance fidelity, because the measurement bias statistics are not characterized during the filtering process.

Covariance fidelity is important for correlation and fusion of tracks provided by multiple sensors [1,2]. Optimistic covariances often cause failures in track-to-track association because covariance uncertainty regions do not overlap. Covariance fidelity may be improved by direct estimation (and removal) of bias parameters in the system dynamics, in the measurements, or in both [3–8]. Depending on the number of bias parameters, algorithms that jointly estimate bias parameters with position and velocity states are computationally intensive, and the system covariance matrix can become numerically ill conditioned, especially when the bias states are poorly observable.

Covariance inflation is a simpler alternative to joint bias estimation. As its description suggests, the uncertainty region is increased (inflated) using mathematical models that approximate the measurement bias effect on position and velocity estimates, thereby improving chances for successful track-to-track association. However, a posteriori covariance inflation does not characterize state-bias correlations that occur during the filtering process.

A bias characterization filter, which is an application of the Schmidt–Kalman filter [9–11], improves covariance fidelity in the presence of sensor measurement biases. As it explicitly models biases in the estimation process, its covariance matrix is more consistent with the statistics of the biased errors in the estimates compared with an extended Kalman filter covariance. It is shown that the bias characterization filter provides the most consistent filter covariance, or best covariance fidelity, compared with several excursions in the Kalman filter, including elevated measurement noise, velocity process noise, and a posteriori covariance inflation. Although similar to considering filtering techniques [12,13], bias characterization is optimal, whereas the former is not.

This Note is organized as follows. A nonlinear bias characterization filter with measurement biases is formulated (Sec. II). Radar measurement and bias models are provided for orbit determination (Sec. III). Nonlinear prediction models for the state, bias, and covariances are formulated from the radar models (Sec. IV). The recursive filter is initialized with an iterated batch filter version of the same algorithm (Sec. V). Satellite orbit determination accuracy and covariance fidelity are demonstrated using Monte Carlo simulations (Sec. VI). Conclusions regarding estimation accuracy and covariance fidelity are provided (Sec. VII).

II. Nonlinear Bias Characterization Filter with Measurement Biases

Unlike a Kalman filter, a bias characterization filter models the effects of measurement biases on state estimates and covariances. A concise derivation of the linear minimum variance filter is provided in the Appendix. In this section, the linear minimum variance filter is generalized to nonlinear problems in the same manner as the extended Kalman filter. Nonlinear expectations are approximated by the lowest-order terms of a series expansion about the current state estimate. Filter estimates and covariances are iterated to improve nonlinear estimation accuracy and covariance fidelity.

For orbit determination, the state vector $\mathbf{x}_n$ at time t_n has six state variables consisting of the components of the Earth-centered inertial (ECI) position $\mathbf{r}_n$ and inertial velocity $\mathbf{v}_n$ of the orbiting object:

$$\mathbf{x}_n = \begin{bmatrix} \mathbf{r}_n \\ \mathbf{v}_n \end{bmatrix}, \qquad \mathbf{r}_n = \begin{bmatrix} x(t_n) \\ y(t_n) \\ z(t_n) \end{bmatrix}, \qquad \mathbf{v}_n = \begin{bmatrix} \dot{x}(t_n) \\ \dot{y}(t_n) \\ \dot{z}(t_n) \end{bmatrix}$$

As sensor measurements $\mathbf{y}_n = \mathbf{h}(\mathbf{x}_n) + M(\mathbf{x}_n)\mathbf{b}_n + \boldsymbol{\upsilon}_n$ are provided in sensor (not inertial) coordinates, the measurement function $\mathbf{h}(\mathbf{x}_n)$, its partial derivative matrix $C(\mathbf{x}_n) = \partial \mathbf{h}_n / \partial \mathbf{x}_n^T$, and the bias sensitivity matrix $M(\mathbf{x}_n)$ are nonlinear functions of $\mathbf{x}_n$. Bias errors $\mathbf{b}_n$ and random measurement errors $\boldsymbol{\upsilon}_n$ are approximated by additive zero-mean uncorrelated Gaussian random variables $E\{\mathbf{b}_n \boldsymbol{\upsilon}_n^T\} = 0$ with variances $B_n = E\{\mathbf{b}_n \mathbf{b}_n^T\}$ and $R_n = E\{\boldsymbol{\upsilon}_n \boldsymbol{\upsilon}_n^T\}$, respectively. These variances can depend on time and, possibly, on the state. These measurement functions and variances are very application-specific (refer to Sec. III for examples).

The random errors $\boldsymbol{\upsilon}_n$ and $\mathbf{b}_n$ fluctuate on different time scales. Sensor noise $\boldsymbol{\upsilon}_n$ fluctuates randomly with each measurement, as in the case of radar thermal noise. Bias errors $\mathbf{b}_n$ fluctuate more slowly, as in the case of a constant attitude reference bias or a slowly varying tropospheric refraction bias. The statistical properties of the biases change over different data collection periods: from hour to hour, day to day, etc.

A nonlinear bias characterization filter with six state variables is denoted by BCF(6). In addition to the state-error covariance $P_n = E\{\delta \mathbf{x}_n \delta \mathbf{x}_n^T\}$, BCF(6) has a state-bias covariance matrix $S_n = E\{\delta \mathbf{x}_n \mathbf{b}_n^T\}$, because state and bias errors are usually correlated. The prior state estimate $\bar{\mathbf{x}}_n$ is updated with the measurement residual $\boldsymbol{\varepsilon}_n$:

$$\hat{\mathbf{x}}_n = \bar{\mathbf{x}}_n + K_n \boldsymbol{\varepsilon}_n$$

$$\boldsymbol{\varepsilon}_n = \mathbf{y}_n - \bar{\mathbf{y}}_n = \mathbf{y}_n - \mathbf{h}(\bar{\mathbf{x}}_n)$$

As $\mathbf{b}_n$ is not estimated, the prior measurement estimate $\bar{\mathbf{y}}_n$ does not include a prior bias estimate. The gain matrix K_n and measurement

Received 5 November 2010; revision received 22 December 2010; accepted for publication 22 December 2010.

*Senior Principal Systems Engineer, 235 Presidential Way. Member AIAA.

residuals covariance N_n depend on two prior covariances: $\bar{P}_n$, and $\bar{S}_n$ (refer to the Appendix for a derivation):

$$K_n = L_n^T N_n^{-1} \qquad L_n = \bar{P}_n \bar{C}_n - \bar{S}_n \bar{M}_n$$
$$N_n = \bar{C}_n \bar{P}_n \bar{C}_n^T + \bar{M}_n B_n \bar{M}_n^T + R_n - \bar{C}_n \bar{S}_n \bar{M}_n^T - \bar{M}_n \bar{S}_n^T \bar{C}_n^T$$

where $\bar{C}_n = C(\bar{\mathbf{x}}_n)$ and $\bar{M}_n = M(\bar{\mathbf{x}}_n)$. The prior covariances are updated using:

$$\hat{P}_n = \bar{P}_n - K_n L_n - (K_n L_n)^T + K_n N_n K_n^T$$

$$\hat{S}_n = (I - K_n \bar{C}_n)\bar{S}_n + K_n \bar{M}_n B_n$$

Linear filtering theory predicts that $\hat{P}_n$ should decrease as more measurements are processed. In many nonlinear applications, the Monte Carlo statistics of the errors in the state estimates are inconsistent with $\hat{P}_n$. Usually, $\hat{P}_n$ is optimistic, meaning that it underestimates the estimation error statistics. Iteration of the estimates and covariances can mitigate filter nonlinearities and improve covariance fidelity. When filter states are sufficiently observable, iteration of the estimates has been shown to approximate a maximum-likelihood estimate using a Gauss–Newton iteration technique [14]. Performance simulations indicate that not more than two or three iterations are needed.

III. Radar Measurement and Bias Models

Phased-array radars provide accurate three-dimensional position measurements in radar range and angle coordinates. Distance (or time delay) is measured relative to the radar, and directional (or angle) measurements are reported in Cartesian radar-face coordinates. These measurements are transformed to ECI coordinates using radar navigation and attitude reference data. For radars on moving platforms, the position, velocity, orientation, and angular rate of the radar array are provided by a strapdown inertial navigation system (INS) mounted on the radar face. Before a mission, the INS is erected to local vertical and aligned north using a conventional gyrocompassing alignment procedure. Radar and INS measurements contain biases as follows.

A phased-array radar using a linear FM (chirp) waveform measures a linear combination $\rho_m = \rho + \tau_{\mathrm{RD}}\dot{\rho}$ of range distance ρ and range rate $\dot{\rho}$. The range-Doppler coupling time τ_{RD} depends on radar center frequency, pulse length, chirp bandwidth, and chirp polarity [15]. As τ_{RD} is known, ρ and $\dot{\rho}$ could be measured directly by transmitting two virtually simultaneous pulses with positive and negative τ_{RD} values. Alternatively, range and range rate can be determined by filtering ρ_m. Range-Doppler radars can also measure Doppler shift, from which $\dot{\rho}$ can be determined, but these radars are not considered here.

Radar angle measurements, which are determined using monopulse techniques [16], provide azimuthal and vertical direction cosines u and v, respectively, of the unit line-of-sight (LOS) vector $\boldsymbol{\lambda}_F$ measured in Cartesian radar-face coordinates:

$$\boldsymbol{\lambda}_F = [\,w \quad u \quad v\,]^T$$

$$w = \sqrt{1 - u^2 - v^2}$$

where w is specified by $|\boldsymbol{\lambda}_F| = 1$. A mechanical control system steers the radar array in azimuth and elevation to maintain an orbiting satellite within a few degrees of radar boresight, and an electronic steering control system centers the radar beam on the object. It follows that $w \equiv 1$, $u = v = 0$, when the LOS is at radar boresight, and $0 < w < 1$ otherwise.

Prior estimates $\bar{\rho}$, $\bar{\dot{\rho}}$, $\bar{u}$, and $\bar{v}$ are determined by transforming the prior state estimate $\bar{\mathbf{x}}$ from ECI to radar-face coordinates using INS data. The transformation $\Re_s(A_s, L_s)$ from ECI to topocentric east-north-up (ENU) coordinates involves the radar right ascension and latitude: A_s and L_s. The transformation $\Re(\phi, \theta, \psi)$ from ENU to radar-face coordinates depends on a yaw angle ψ measured from the east in the local horizontal plane, a pitch angle θ measured up from the local horizontal to the radar boresight, and a roll angle ϕ measured around the radar boresight. The INS orientation angles ψ, θ, and ϕ contain biases. Horizontal (north-pointing) misalignments cause a yaw bias $\delta\psi$, whereas vertical misalignments cause a pitch bias $\delta\theta$ and a roll bias $\delta\phi$.

In radar-face spherical coordinates, the radar measurement $\mathbf{y}$ is corrupted by an additive measurement bias and random errors:

$$\mathbf{y} = \begin{bmatrix} \rho + \tau_{\mathrm{RD}}\dot{\rho} \\ u \\ v \end{bmatrix} + \begin{bmatrix} \delta\rho \\ \delta u \\ \delta v \end{bmatrix} + \boldsymbol{\upsilon}$$

The range bias $\delta\rho$ and angle biases, δu and δv, are modeled by static and dynamic error components in radar-face coordinates (to be discussed shortly). Zero-mean Gaussian random errors $\boldsymbol{\upsilon}$ have a diagonal measurement noise matrix R:

$$R = E\{\boldsymbol{\upsilon}\boldsymbol{\upsilon}^T\} = \mathrm{diag}\{\,\sigma^2_{\rho+\tau\dot{\rho}} \quad \sigma_u^2 \quad \sigma_v^2\,\}$$

where $\sigma_{\rho+\tau\dot{\rho}}$ is comparable to the navigation bias, and σ_u and σ_v are comparable to the orientation biases. It is important that $\mathbf{y}$ is independent of the INS orientation biases.

Static or time-invariant biases include constant biases $\delta\rho_B$, δu_B, and δv_B, scale factor biases κ_ρ, κ_u, and κ_v, multiplying the respective measurements, and a clock error $\delta\varphi$ measured around the radar boresight. Constant biases are usually removed during the premission radar calibration process. Although scale factor and clock-error biases can cause significant u and v biases at large scan angles from the boresight, these errors may be neglected when the radar LOS is near boresight, corresponding to $u, v \approx 0$. As static biases can be neglected for the reasons stated, the radar measurement biases are dominated by the dynamic biases.

Dynamic bias errors arise primarily from electromagnetic ray propagation through the troposphere. Tropospheric propagation causes delays in the round-trip travel time and angular refraction errors that fluctuate with LOS elevation γ and with local atmospheric conditions along the radar path to a satellite [17–19]. Although refraction errors can be compensated with tropospheric models, residual (or uncompensated) delays cause range errors $\delta\rho$, and residual angular refraction errors cause errors $\delta\gamma$ and $\delta\alpha$ in LOS elevation γ and azimuth α. Dynamic bias errors may be expressed in matrix form [8]:

$$\begin{bmatrix} \delta\rho \\ \delta u \\ \delta v \end{bmatrix} = \Theta^{-1}\Re(\phi, \theta, \psi)\Lambda(\rho, \gamma, \alpha)\delta\boldsymbol{\eta}$$

$$\delta\boldsymbol{\eta} = [\,\delta\rho \quad \delta\alpha \quad \delta\gamma\,]^T$$

$$\Lambda(\rho, \gamma, \alpha) = \begin{bmatrix} \cos\gamma\sin\alpha & \rho\cos\gamma\cos\alpha & -\rho\sin\gamma\sin\alpha \\ \cos\gamma\cos\alpha & -\rho\cos\gamma\sin\alpha & -\rho\sin\gamma\cos\alpha \\ \sin\gamma & 0 & \rho\cos\gamma \end{bmatrix}$$

$$\Theta = \begin{bmatrix} w & -\rho u/w & -\rho v/w \\ u & \rho & 0 \\ v & 0 & \rho \end{bmatrix}$$

Radar measurement biases $\delta\boldsymbol{\eta}$ are modeled by a linear first-order vector Markov process with a variable time constant τ_A and zero-mean Gaussian disturbance input $\delta\mathbf{f}$:

$$\frac{\mathrm{d}}{\mathrm{d}t}(\delta\boldsymbol{\eta}) + \frac{1}{\tau_A}\delta\boldsymbol{\eta} = \frac{1}{\tau_A}\delta\mathbf{f}$$

$$E\{\delta\mathbf{f}\} = \mathbf{0}_3, \qquad E\{\delta\mathbf{f}\delta\mathbf{f}^T\} = \text{diag}\{\, q_\rho \quad q_\alpha \quad q_\gamma \,\}$$

Although $\delta\mathbf{f} = 0$ for state prediction, constant variances q_ρ, q_α, and q_γ (refer to Table 1) may be interpreted as process noise commands to the Markov bias covariance model. The Markov time constant τ_A varies with LOS elevation γ, with elevation rate $\dot{\gamma}$, and with the elevation-dependent refraction error $\varepsilon(\gamma)$ and its elevation gradient (refer to Fig. 1):

$$\tau_A = -\varepsilon(\gamma)/(\dot{\gamma}\, d\varepsilon/d\gamma)$$

As $d\varepsilon/d\gamma < 0$, stable error dynamics ($\tau_A > 0$) occur with increasing elevation ($\dot{\gamma} > 0$), and unstable error dynamics ($\tau_A < 0$) occur with decreasing elevation ($\dot{\gamma} < 0$). As τ_A is undefined at peak elevation ($\dot{\gamma} = 0$), a maximum $|\tau_A|$ value (1000 s) is assigned to avoid singularities.

Orientation biases $\delta\boldsymbol{\xi} = [\,\delta\psi \quad \delta\theta \quad \delta\phi\,]^T$ fluctuate as the radar array (on which the INS is mounted) follows the satellite trajectory in elevation and azimuth. Differential equations may be derived by linearization of the Euler equations specifying the angular rates [8]:

$$\frac{\mathrm{d}}{\mathrm{d}t}(\delta\boldsymbol{\xi}) = \Gamma(\theta,\phi)\delta\boldsymbol{\xi} + \Im^{-1}\delta\boldsymbol{\omega}_s$$

$$\Im^{-1}(\theta,\phi) = \frac{1}{\cos\theta}\begin{bmatrix} 0 & \sin\phi & \cos\phi \\ 0 & -\cos\theta\cos\phi & \cos\theta\sin\phi \\ \cos\theta & -\sin\theta\sin\phi & -\sin\theta\cos\phi \end{bmatrix}$$

$$\Gamma(\theta,\phi,\boldsymbol{\omega}_s) = \begin{bmatrix} \frac{\partial\Im^{-1}}{\partial\psi}\boldsymbol{\omega}_s & \frac{\partial\Im^{-1}}{\partial\theta}\boldsymbol{\omega}_s & \frac{\partial\Im^{-1}}{\partial\phi}\boldsymbol{\omega}_s \end{bmatrix}$$

$$\frac{\partial\Im^{-1}}{\partial\psi} = O_3$$

$$\frac{\partial\Im^{-1}}{\partial\theta} = \frac{1}{\cos\theta}\begin{bmatrix} 0 & 0 & 0 \\ 0 & \sin\theta\cos\phi & -\sin\theta\sin\phi \\ -\sin\theta & -\cos\theta\sin\phi & -\cos\theta\cos\phi \end{bmatrix} + \tan\theta\,\Im^{-1}$$

$$\frac{\partial\Im^{-1}}{\partial\phi} = \frac{1}{\cos\theta}\begin{bmatrix} 0 & \cos\phi & -\sin\phi \\ 0 & \cos\theta\sin\phi & \cos\theta\cos\phi \\ 0 & -\sin\theta\cos\phi & \sin\theta\sin\phi \end{bmatrix}$$

where $\boldsymbol{\omega}_s$ is the Earth-relative angular rate in radar-face coordinates. The angular rate bias $\delta\boldsymbol{\omega}_s$ is a zero-mean Gaussian random vector:

$$E\{\delta\boldsymbol{\omega}_s\} = \mathbf{0}_3, \qquad E\{\delta\boldsymbol{\omega}_s\delta\boldsymbol{\omega}_s^T\} = \begin{bmatrix} q_\omega & 0 & 0 \\ 0 & q_\omega & 0 \\ 0 & 0 & q_\omega \end{bmatrix}$$

where process noise statistics for the misalignment biases are provided in Table 1.

The prior estimate of the measurement is specified by:

$$\bar{\mathbf{y}} = \begin{bmatrix} \bar{\rho} + \tau_{\mathrm{RD}}\dot{\bar{\rho}} \\ \bar{u} \\ \bar{v} \end{bmatrix} + M(\bar{\mathbf{x}},\psi,\theta,\phi)\begin{bmatrix} \delta\bar{\boldsymbol{\xi}} \\ \delta\bar{\boldsymbol{\eta}} \end{bmatrix}$$

$$M(\mathbf{x},\psi,\theta,\phi) = [\,-J_\xi \quad \Theta^{-1}\Re(\phi,\vartheta,\psi)\Lambda(\rho,\gamma,\alpha)\,]$$

The measurement sensitivity matrix is determined by partial differentiations of the bias-free prior measurement function with respect to the orbit state variables:

$$C(\mathbf{x}) = \frac{\partial(\rho + \tau_{\mathrm{RD}}\dot{\rho}, u, v)}{\partial(x, y, z, \dot{x}, \dot{y}, \dot{z})}$$

Partial derivatives are selected from the appropriate rows and columns of the 4×3 Jacobian transformation matrices:

$$\frac{\partial(\rho, w, u, v)}{\partial(x, y, z)} = \frac{\partial(\dot{\rho}, \dot{w}, \dot{u}, \dot{v})}{\partial(\dot{x}, \dot{y}, \dot{z})} = \begin{bmatrix} \boldsymbol{\lambda}_F^T\Re(\phi,\vartheta,\psi)\Re_s(A_s, L_s) \\ \frac{1}{\rho}(I_3 - \boldsymbol{\lambda}_F\boldsymbol{\lambda}_F^T)\Re(\phi,\vartheta,\psi)\Re_s(A_s, L_s) \end{bmatrix}$$

Elements of the orientation bias sensitivity matrix

$$J_\xi = \partial(\rho + \tau_{\mathrm{RD}}\dot{\rho}, u, v)/\partial(\psi, \theta, \phi)$$

are selected from the appropriate rows of the 4×3 Jacobian matrix:

$$\frac{\partial(\rho + \tau_{\mathrm{RD}}\dot{\rho}, w, u, v)}{\partial(\psi, \theta, \phi)} = \begin{bmatrix} -\frac{1}{2}\rho[\,\cos^2\theta\delta\psi \quad \delta\theta \quad 0\,] \\ \Omega(\boldsymbol{\lambda}_F)\Im(\theta,\phi) \end{bmatrix}$$

$$\Im(\theta,\phi) = \begin{bmatrix} \sin\theta & 0 & 1 \\ \cos\theta\sin\phi & -\cos\phi & 0 \\ \cos\theta\cos\phi & \sin\phi & 0 \end{bmatrix}$$

where $\Omega(*)$ is the skew-symmetric rotation matrix. Orientation biases cause second-order range corrections, because $\bar{\rho}$ is projected onto a misaligned unit LOS direction. As range is independent of orientation to the first order, this second-order term is always negative [i.e., because it is analogous to a $\cos(\bullet) - 1$ term]. This second-order term provides mathematical observability of the orientation biases for bias estimation, but it has a negligible effect on estimation accuracy unless highly precise range measurements are available. The $J_\xi\delta\bar{\boldsymbol{\xi}}$ term is subtracted[†] (rather than added) in order that $\bar{\mathbf{y}}$ be independent of $\delta\bar{\boldsymbol{\xi}}$ before computation of the measurement residual [8].

IV. Prediction Models for Bias Characterization Filter

Estimates and covariances are generated using a sequential prediction and correction process. In this section, nonlinear filter prediction models are formulated for orbit and bias states. At the first update, initial conditions for the state and covariance are provided by a batch filter (refer to Sec. V).

At altitudes above 500 km, where drag is not important, orbital motion is described by

$$\frac{\mathrm{d}\mathbf{r}}{\mathrm{d}t} = \mathbf{v}$$

$$\frac{\mathrm{d}\mathbf{v}}{\mathrm{d}t} = -\frac{\mu_e}{r^2}\left\{\frac{\mathbf{r}}{r} - \frac{3J_2R_e^2}{2r^2}\left[\left(\frac{5z^2}{r^2} - 1\right)\frac{\mathbf{r}}{r} - \frac{2z}{r}\hat{Z}\right]\right\} + \nabla U$$

where μ_e, R_e, and $\hat{Z}$ are the Earth's gravitational parameter, equatorial radius, and unit-polar axis, respectively, and time derivatives are taken with respect to the ECI frame. The dominant gravitational accelerations arise from the central inverse-square gravity field and from Earth oblateness (modeled by the J_2 coefficient). As each higher-order zonal or tesseral harmonic term of the geopotential function U is $\mathcal{O}(J_2^2)$, the higher-order disturbing acceleration ∇U is, at most, 15–20 μg at orbital altitudes of 700 km, depending on the geographic location of the subsatellite point. For short data collection and prediction intervals (e.g., 1000 s), ∇U may be neglected. Prediction equations for the state-error covariance are given by

[†]Equivalently, this term could be added to $\mathbf{y}$ instead (because it is otherwise independent of orientation biases) when the measurement residual is formed.

$$\frac{\mathrm{d}P}{\mathrm{d}t} = F(\mathbf{x})P + PF(\mathbf{x})^T$$

$$F(\mathbf{x}) = \begin{bmatrix} O_3 & I_3 \\ \Gamma_g & O_3 \end{bmatrix}$$

$$\Gamma_g = \frac{\mu_e}{r^3}\left(\frac{3\mathbf{r}\mathbf{r}^T}{r^2} - I_3\right) + \frac{3\mu_e J_2 R_e^2}{2r^5}\Gamma_2$$

$$\Gamma_2 = \begin{bmatrix} \frac{5(x^2+z^2)}{r^2} - \frac{35x^2z^2}{r^4} - 1 & \frac{5xy}{r^2} - \frac{35xyz^2}{r^4} & \frac{15xz}{r^2} - \frac{35xz^3}{r^4} \\ \frac{5xy}{r^2} - \frac{35xyz^2}{r^4} & \frac{5(y^2+z^2)}{r^2} - \frac{35y^2z^2}{r^4} - 1 & \frac{15yz}{r^2} - \frac{35yz^3}{r^4} \\ \frac{15xz}{r^2} - \frac{35xz^3}{r^4} & \frac{15yz}{r^2} - \frac{35yz^3}{r^4} & \frac{30z^2}{r^2} - \frac{35z^4}{r^4} - 3 \end{bmatrix}$$

where the gravity-gradient matrix Γ_g is complete to $\mathcal{O}(J_2)$. After the first update with the batch filter, initial conditions for state and covariance predictions are provided by the BCF(6) updates $\hat{x}_n$ and $\hat{P}_n$ (refer to Sec. II). Process noise is not included in the state prediction equations. Instead, process noise will be included in the bias covariance prediction model as follows.

The bias-state vector $\mathbf{b}$ includes orientation biases and radar measurement biases, discussed in the previous section:

$$\mathbf{b} = \begin{bmatrix} \delta\boldsymbol{\xi}(t) \\ \delta\boldsymbol{\eta}(t) \end{bmatrix}, \qquad \delta\boldsymbol{\xi} = \begin{bmatrix} \delta\psi \\ \delta\theta \\ \delta\phi \end{bmatrix}, \qquad \delta\boldsymbol{\eta} = \begin{bmatrix} \delta\rho \\ \delta\alpha \\ \delta\gamma \end{bmatrix}$$

Prediction equations for the bias states and bias covariance are given by

$$\frac{\mathrm{d}\mathbf{b}}{\mathrm{d}t} = F_B\mathbf{b}$$

$$\frac{\mathrm{d}B}{\mathrm{d}t} = F_B B + BF_B^T + G_B Q_B G_B^T$$

$$F_B = \begin{bmatrix} \Gamma(\theta,\phi) & O_3 \\ O_3 & -I_3/\tau_A \end{bmatrix}$$

$$G_B = \begin{bmatrix} \Im^{-1} & O_3 \\ O_3 & I_3/\tau_A \end{bmatrix}$$

$$Q_B = \mathrm{diag}\{\, q_\omega \quad q_\omega \quad q_\omega \quad q_\rho \quad q_\alpha \quad q_\gamma \,\}$$

where zero-mean process noise is not modeled in the prediction of $\mathbf{b}$. Process noise Q_B is included in the covariance prediction of B (refer to Table 1). As $\mathbf{b}$ and B are characterized but not updated, initial conditions for the bias state and covariance are provided by the prior bias and covariance from the previous integration step. Zero initial conditions are assumed, except for the INS misalignment components of B (refer to Table 2).

Table 1 Tropospheric and angular velocity bias process noise models

Bias process noise source	Symbol	Value
Tropospheric range delay bias	q_ρ	$(2.5\ \mathrm{m})^2$
Tropospheric azimuth refraction bias	q_α	$(250\ \mu\mathrm{rad})^2$
Tropospheric elevation refraction bias	q_γ	$(500\ \mu\mathrm{rad})^2$
INS angular velocity process noise (each axis)	q_ω	$(0.5\ \mu\mathrm{rad/s})^2$

Table 2 INS misalignment statistics

Description	Symbol	Value
Initial uncertainty in yaw alignment	$\sigma_\psi(0)$	150 μrad
Initial uncertainty in pitch alignment	$\sigma_\theta(0)$	80 μrad
Initial uncertainty in roll alignment	$\sigma_\phi(0)$	80 μrad

The prediction equation for the bias-state correlation covariance matrix is given by

$$\frac{\mathrm{d}S}{\mathrm{d}t} = FS + SF_B^T$$

After the first update with the batch filter, initial conditions are provided by the BCF(6) update $\hat{S}_n$ (refer to Sec. II).

V. Iterated Batch Filter for Initialization

The recursive BCF(6) may be initialized using measurements collected over the time interval $t_n \in [t_0, t_N]$. An initial prior state estimate $\bar{\mathbf{x}}_0$ and covariance $\bar{P}_0$ may be determined with a polynomial batch filter having locally linear dynamics in the measurement variables. The smoothed measurement estimates and covariance are transformed to $\bar{\mathbf{x}}_0$ and $\bar{P}_0$ using coordinate transformations and kinematic models. A zero initial condition is assumed for the state-bias covariance ($\bar{S}_0 = 0$), because the state and bias errors are initially uncorrelated. Estimates and covariances are predicted to the current measurement time t_n using a nonlinear prediction model:

$$\bar{\mathbf{x}}_n = \Phi(\bar{\mathbf{x}}_0, t_n - t_0)\bar{\mathbf{x}}_0$$

$$\bar{P}_n = \Phi(\bar{\mathbf{x}}_0, t_n - t_0)\bar{P}_0\Phi^T(\bar{\mathbf{x}}_0, t_n - t_0)$$

$$\bar{S}_n = \Phi(\bar{\mathbf{x}}_0, t_n - t_0)\bar{S}_0\Psi^T(t_n - t_0)$$

An analytic solution for the nonlinear state-transition matrix Φ exists for Keplerian orbits [20]. For higher-order gravity models, Φ is the solution of the following matrix-differential equation:

$$\frac{\mathrm{d}\Phi}{\mathrm{d}t} = F(\mathbf{x})\Phi, \qquad \Phi(0) = I_6$$

which is coupled to the state prediction equation because F depends on the state (Sec. IV). Similarly, the bias transition matrix Ψ is the solution of another matrix-differential equation:

$$\frac{\mathrm{d}\Psi}{\mathrm{d}t} = F_B(\theta, \phi, \tau_A)\Psi, \qquad \Psi(0) = I_6$$

where F_B depends on the radar orientation angles θ and ϕ, and the (time dependent) Markov time constant τ_A for tropospheric effects (Fig. 1). At time t_n, the transition matrix solutions $\Phi(\bar{\mathbf{x}}_0, t_n - t_0)$ and $\Psi(t_n - t_0)$ are explicit functions of elapsed time $t_n - t_0$ and the prior initial state $\bar{\mathbf{x}}_0$, and they are implicit functions of auxiliary parameters for the tropospheric model.

A weighted least-squares estimate $\hat{\mathbf{x}}_0$ is generated at the sensor acquisition time t_0 using

$$\hat{\mathbf{x}}_0 = \bar{\mathbf{x}}_0 + \left[\sum_n (G_n^T N_n^{-1} G_n)\right]^{-1} \sum_n G_n^T N_n^{-1}\boldsymbol{\varepsilon}_n$$

$$\boldsymbol{\varepsilon}_n = \mathbf{y}_n - \mathbf{h}(\bar{\mathbf{x}}_n)$$

$$N_n = G_n\bar{P}_0G_n^T - G_n\bar{S}_0F_n^T - F_n\bar{S}_0^TG_n^T + F_nB_0F_n^T + R_n$$

where the observability gramian matrices G_n and F_n are specified by

$$G_n = \bar{C}_n\Phi(\bar{\mathbf{x}}_0, t_n - t_0)$$

$$F_n = \bar{M}_n\Psi(t_n - t_0)$$

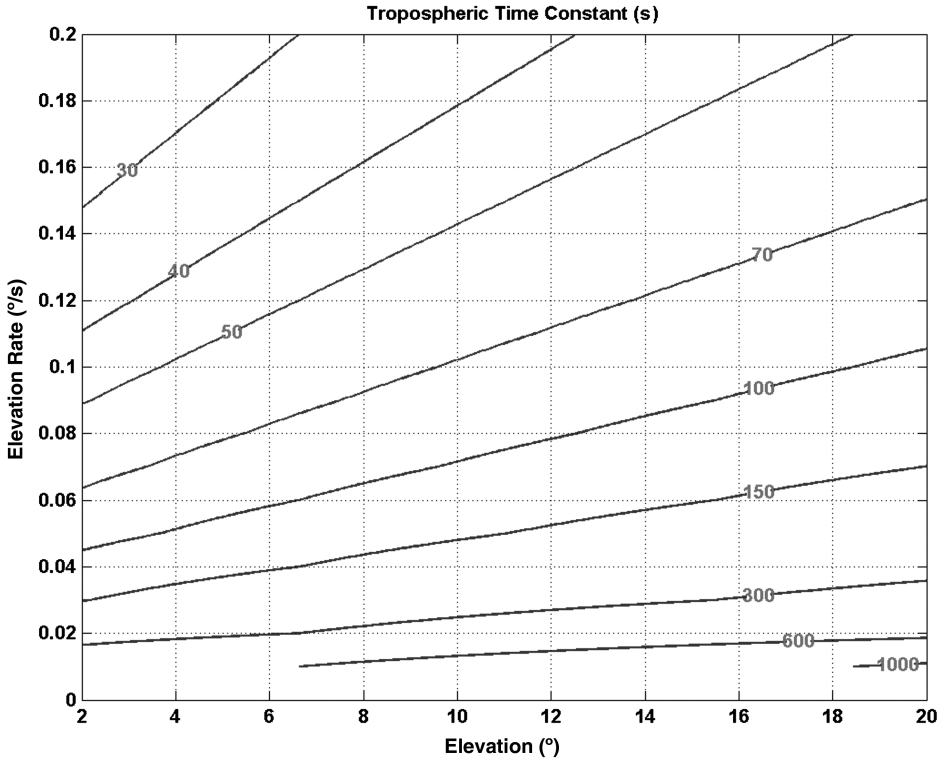

Fig. 1 Markov (absolute) time constant for clear air tropospheric disturbances.

In these equations, summations are taken over all associated measurements, and the measurement sensitivity matrices $\bar{C}_n = C(\bar{\mathbf{x}}_n)$ and $\bar{M}_n = M(\bar{\mathbf{x}}_n)$ were given earlier (Sec. III). The covariance update may be expressed in matrix form:

$$\hat{P}_0 = \left[\sum_n (G_n^T N_n^{-1} G_n)\right]^{-1} \left[\sum_n G_n^T N_n^{-1} (F_n B_0 F_n^T + R_n) N_n^{-1} G_n\right] \left[\sum_n (G_n^T N_n^{-1} G_n)\right]^{-1}$$

$\hat{P}_0$ is not explicitly dependent on the prior covariance $\bar{P}_0$. Rather, $\bar{P}_0$ is implicit in the diagonal elements of W because the residuals covariance N_n depends on $\bar{P}_0$.

Estimation accuracy and covariance fidelity may be improved by iterating the weighted least-squares estimate and covariance in a similar fashion as the recursive process (Sec. II). On each iteration, the nonlinear measurement functions are evaluated with improved estimates. Simulations suggest that no more than three to five iterations are needed and that measurements should be collected for at least 10–15 s (at 1 Hz data rate) for proper covariance conditioning.

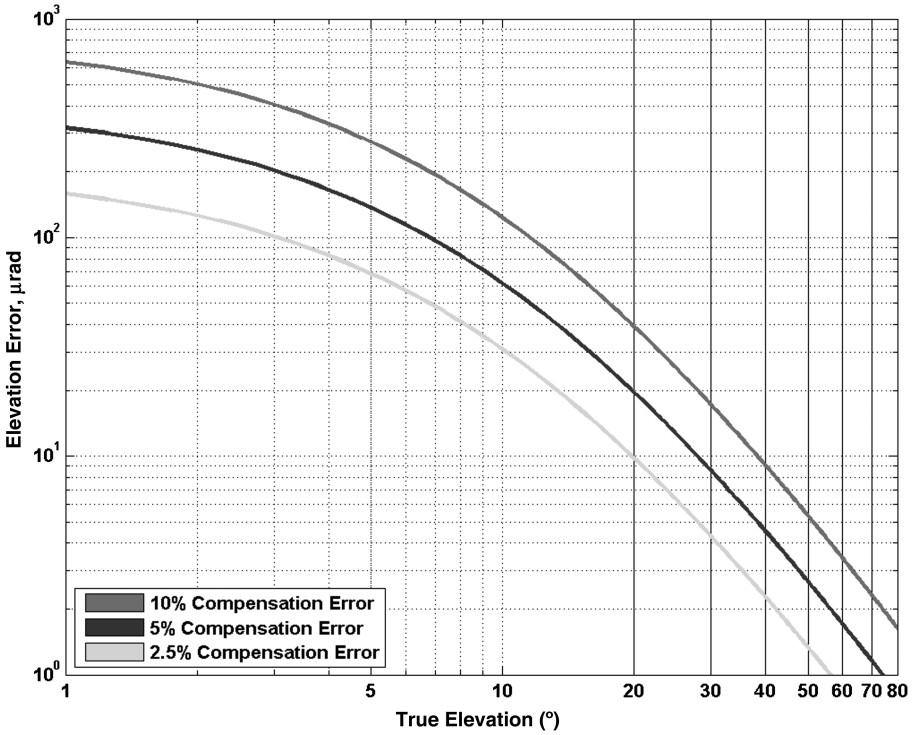

Fig. 2 Elevation measurement biases caused by uncompensated clear air tropospheric refraction (no weather effects). Real-time calibration models typically correct 90–95% of the error, leaving 5–10% residual (or uncompensated) errors (3σ).

Table 3 Gauss–Markov tropospheric weather disturbance model

Description	Symbol	Value
Gauss–Markov time constant	τ_w	50 s
Range variance	$\tilde{q}_\rho$	$(5\ \text{m})^2$
Azimuth and elevation variances	$\tilde{q}_{\alpha\gamma}$	$(500\ \mu\text{rad})^2$

VI. Orbit Determination Accuracy and Covariance Fidelity

BCF(6) performance is demonstrated by the Monte Carlo simulation. A ground-based tracking radar provides 20 dB signal-to-noise ratio on a spherical satellite in a near-circular orbit with altitude 1500 km. As the satellite traverses the sky, the phased array rotates in azimuth and elevation in order to maintain the satellite at or near the radar boresight. Radar position, velocity, orientation, and angular rate are provided by an INS mounted on the phased array, near boresight. For high range and angle resolution radars, radar measurement and INS misalignment biases dominate orbit determination accuracies.

Radar range and angle biases arise from uncompensated tropospheric refraction errors. Real-time corrections to range and elevation are usually computed using in situ measurements of pressure, temperature, and relative humidity. However, these corrections remove all but 5 to 10% (3σ) of the total refraction errors, leaving residual measurement biases. In clear air environments (no weather effects), tropospheric elevation errors scale with elevation, and the largest errors occur at low elevations (below 5°; refer to Fig. 2).

In weather environments, clouds can cause time-dependent refraction errors in range, azimuth, and elevation $\delta\boldsymbol{\eta}_w = [\delta\rho_w \quad \delta\alpha_w \quad \delta\gamma_w]^T$. These disturbances are modeled by colored noise, or by Gauss–Markov random processes with time constant τ_w and zero-mean forcing function $\delta\mathbf{f}_w$:

$$\frac{\mathrm{d}}{\mathrm{d}t}(\delta\boldsymbol{\eta}_w) + \frac{1}{\tau_w}\delta\boldsymbol{\eta}_w = \frac{1}{\tau_w}\delta\mathbf{f}_w$$

$$E\{\delta\mathbf{f}_w\} = \mathbf{0}_3, \qquad E\{\delta\mathbf{f}_w\delta\mathbf{f}_w^T\} = \mathrm{diag}\{\,\tilde{q}_\rho \quad \tilde{q}_{\alpha\gamma} \quad \tilde{q}_{\alpha\gamma}\,\}$$

Numerical values of the Gauss–Markov parameters are provided in Table 3.

Covariance histories of the weather disturbances, based on the preceding Gauss–Markov model, and the INS misalignment biases are shown in Fig. 3. INS misalignments are based on the linearized Euler equations and the bias initial condition statistics provided in Table 2. Although ensemble (e.g., day to day) 1σ bias statistics do not fluctuate significantly during a satellite pass, single-trial misalignment errors can fluctuate significantly as the radar boresight follows the satellite across the sky (not shown).

Random and bias measurement errors were randomized in the Monte Carlo analysis. Clear air refraction errors are modeled by random scale factors on the elevation profile in Fig. 2. Weather refraction errors are modeled by a Gauss–Markov random process, with parameters and statistics given in Table 3. INS misalignments are modeled as random initial conditions, with statistics provided in Table 2. Although orbit parameters were not randomized, filter initial conditions were randomly generated by processing the randomly corrupted radar measurements with the iterated batch filter discussed in Sec. V. This approach assures good consistency of the initial errors in the estimates and filter covariances, as the results will indicate.

As biases are not actively estimated or corrected, the 1σ Monte Carlo position and velocity error statistics versus truth are nearly the same for the BCF(6) filter (Fig. 4) and the corresponding extended Kalman filter, or EKF(6) (Fig. 5). Angular errors cause orbit determination errors in position and velocity. Crossrange position (relative to the LOS) errors scale with the product of satellite range and angle error, whereas crossrange velocity errors scale with the product of range rate and angle error. As radar measurements are taken in a rotating antenna frame, Coriolis effects cause range rate errors that scale with the product of satellite range, angle error, and LOS angular rate.

Tropospheric delay and angular refraction errors are most pronounced at low elevations (below 5°), occurring early and late in the track. These errors are most pronounced early in the track when the filter gains are highest. The filter has better disturbance rejection late

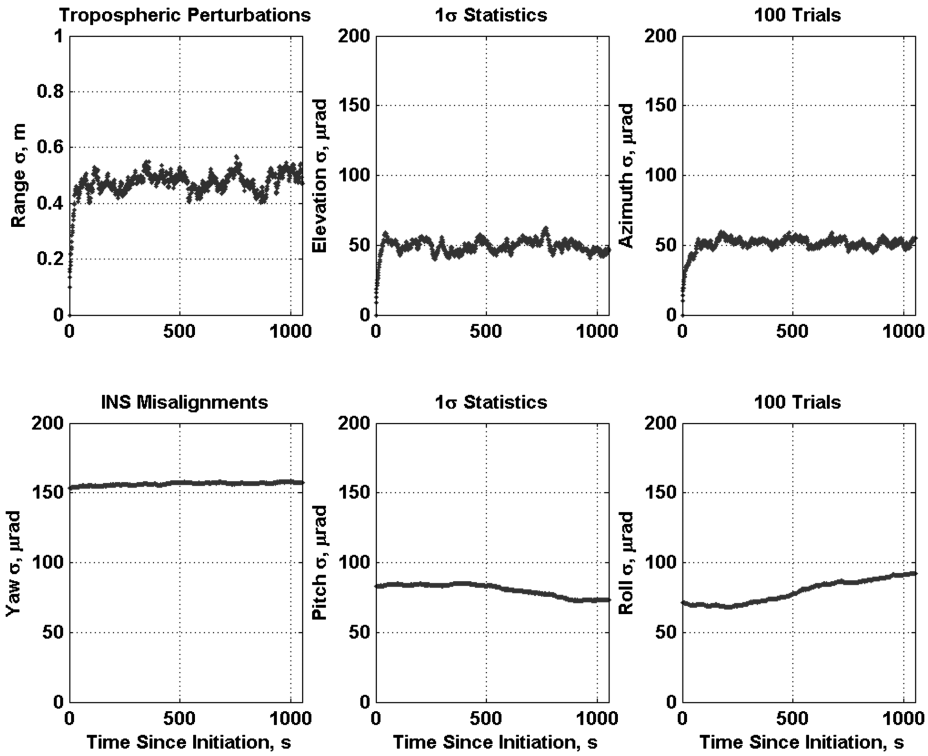

Fig. 3 1σ Bias statistics for Gauss–Markov tropospheric weather model (top row) and inertial navigation system misalignments (bottom row) based on 100 Monte Carlo trials.

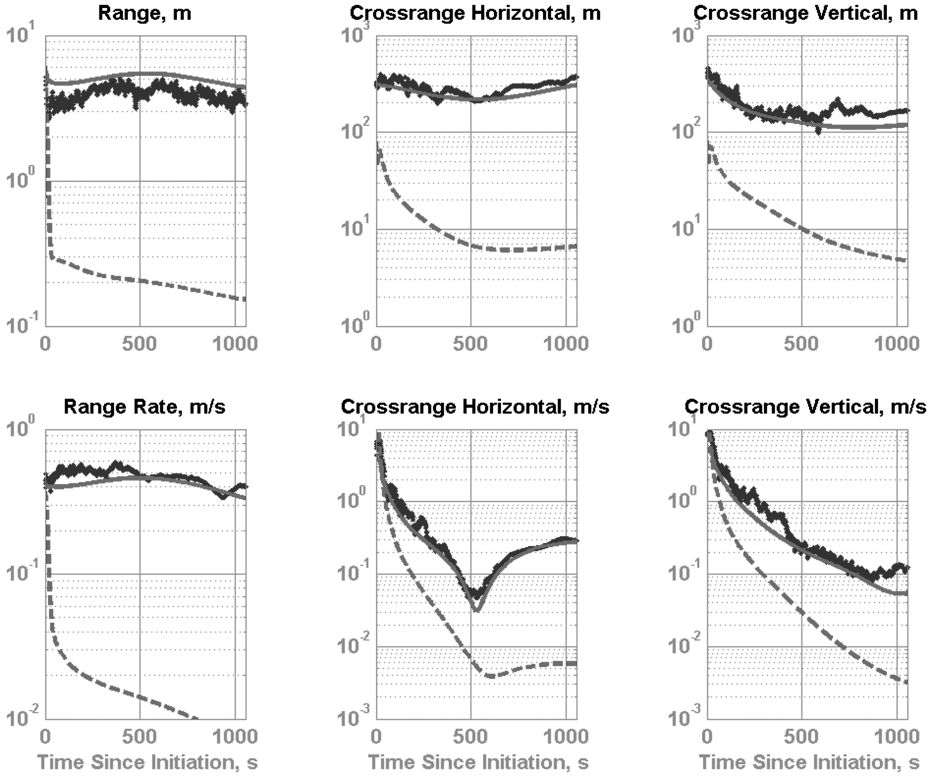

Fig. 4 Bias characterization filter 1σ estimation errors vs truth (irregular lines) and covariance traces (smooth lines) based on 100 Monte Carlo trials (baseline Kalman filter covariance traces shown by dashed lines).

in the track, after the filter gains have diminished. Although INS angular misalignments are always present, their effects become more evident at higher elevations (above 20°) during the midtrack interval, when the tropospheric effects are diminished.

As expected, the BCF(6) covariance is much more consistent with its estimation error statistics (Fig. 4), indicating that this filter provides much better estimates of its own errors than EKF(6). Baseline EKF(6) covariances grossly underestimate the Monte Carlo

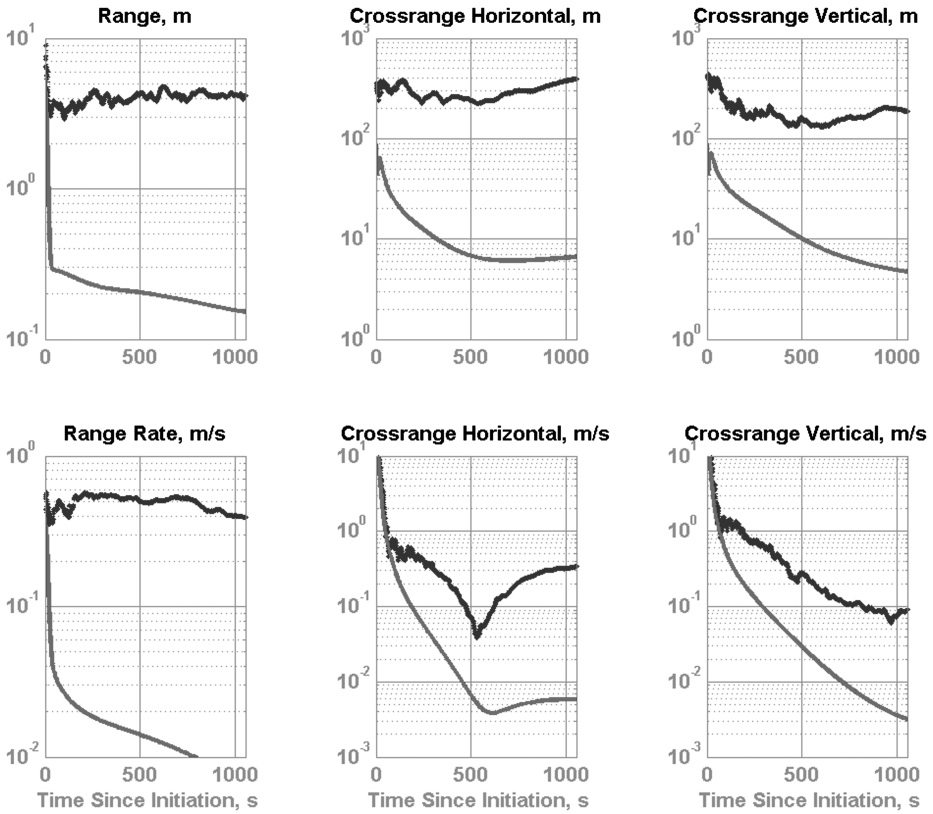

Fig. 5 Baseline extended Kalman filter 1σ estimation errors vs truth (irregular lines) and covariance traces (smooth lines) based on 100 Monte Carlo trials.

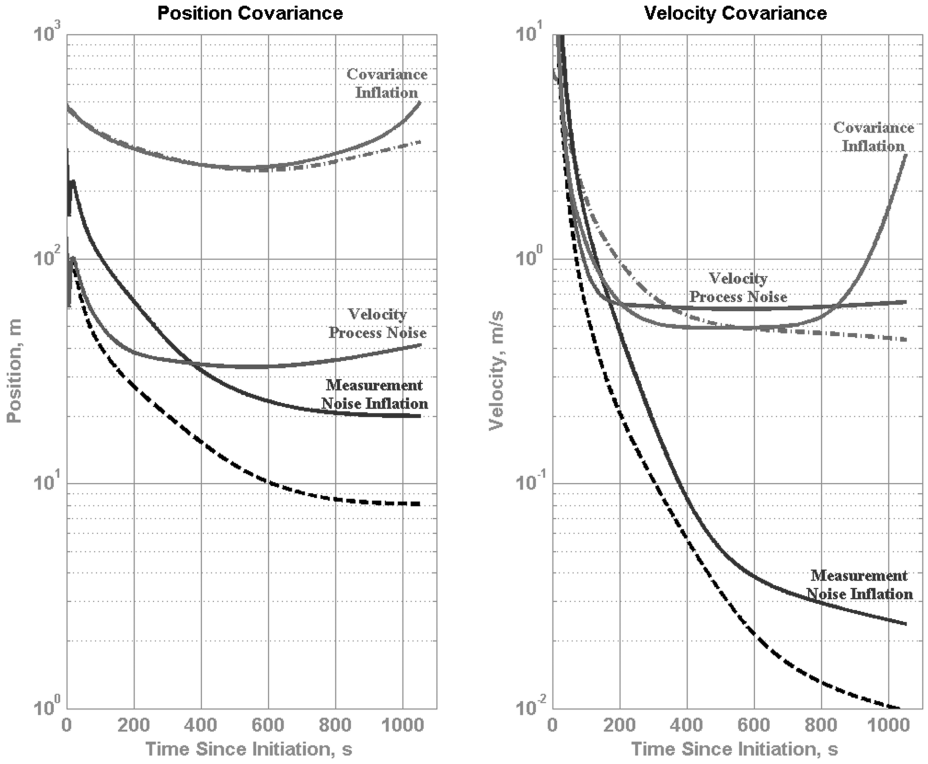

Fig. 6 1σ covariance traces for measurement noise inflation, velocity process noise, and a posteriori covariance inflation (labeled solid curves) are compared with baseline Kalman filter (dashed curve) and bias characterization filter (chain dashed curve).

error statistics by at least an order of magnitude (dashed line in Fig. 4).

Several excursions of the baseline EKF(6) parameters were tried in order to improve covariance fidelity (Fig. 6). Elevated levels of range and angle measurement noise are relatively ineffective. This should not be surprising, because Kalman filters are designed to attenuate random measurement errors, and the noise-inflated covariance attenuates quickly after filter initiation. Nonzero velocity process noise improves velocity covariance, but position covariance remains optimistic. It is interesting that process noise, which usually compensates for unmodeled accelerations, emulates an unmodeled sensor bias error's effect on velocity accuracy. Finally, sensor bias models can be used for a posteriori covariance inflation. Covariances are successfully inflated early in the track, but covariance fidelity degrades by the end of track. As it does not model the interaction of the filtering process with the sensor bias, covariance inflation cannot and does not properly model the disturbance rejection response of the filter to the tropospheric bias. Consequently, the inflated covariances trend upward at both ends of the track.

BCF(6) provides the most reliable orbit determination accuracy, showing that it has excellent covariance fidelity. Surprisingly, process noise can be selectively tuned to emulate the effects of sensor bias, but this approach is only effective in postmission analysis (after the fact). For real-time implementation in missile defense scenarios, many factors must be taken into consideration, such as observation geometry. With BCF(6), physics-based models of the bias and bias statistics successfully capture these complicated interactions.

VII. Conclusions

BCF(6) improves covariance fidelity in the presence of sensor measurement biases. As it explicitly models biases in the estimation process, the BCF(6) covariance matrix is more consistent with the statistics of the biased errors in the estimates compared with the extended Kalman filter, or EKF(6), covariance matrix, which does not have bias characterization.

Monte Carlo simulations of a radar orbit determination with sensor biases show that the baseline EKF(6) covariance can be optimistic by an order of magnitude compared with the BCF(6) covariance. Several ad hoc techniques for improvement of the EKF(6) covariance fidelity are not effective or suitable for real-time implementation. For example, velocity process noise, if properly tuned after the fact, can improve EKF(6) velocity covariance, but position covariances are significantly mismatched. Process noise tuning is more suitable for postmission reconstruction. Covariance inflation improves position and velocity covariance fidelity early in the track, but fidelity degrades after extended periods in the track. Finally, elevated levels of measurement noise covariance are ineffective because bias errors cannot be modeled as random errors. For example, EKF(6) attenuates random errors but not sensor bias errors.

Bias characterization is clearly the most effective real-time method for improvement of covariance fidelity. Physics-based models for the bias and bias statistics properly account for sensor biases in the filtering process, whereas other methods do not. Consequently, bias characterization is suitable for correlation and fusion of tracks provided by multiple sensors, and it is suitable for battle management and weapon access decisions that require reliable real-time track accuracy.

Appendix: Derivation of Linear Minimum Variance Filter

A concise derivation is presented of the linear, minimum variance filter gain K, using the matrices defined in Sec. II. Following Schmidt [10], an optimal state estimate $\hat{\mathbf{x}}$ is a linear function of the prior estimate $\bar{\mathbf{x}}$ and the measurement such that $\hat{\mathbf{x}} = \bar{\mathbf{x}} + K(\mathbf{y} - \bar{\mathbf{y}})$. Following substitution of $\mathbf{y} = C\mathbf{x} + M\mathbf{b} + \boldsymbol{\nu}$ and $\bar{\mathbf{y}} = C\bar{\mathbf{x}}$, the error in the optimal estimate may be expressed by $\delta\hat{\mathbf{x}} = (I - KC)\delta\bar{\mathbf{x}} + KM\mathbf{b} + K\boldsymbol{\nu}$. The expectation of the product $\delta\hat{\mathbf{x}}\delta\hat{\mathbf{x}}^T$ yields the following relationship between $\hat{P}$ and K:

$$\hat{P} = (I - KC)\bar{P}(I - KC)^T + (I - KC)\bar{S}(KM)^T + KM\bar{S}^T(I - KC)^T + K(MBM^T + R)K^T$$

where the random error is uncorrelated with the bias and with the prior error in the estimate, such that $E\{\mathbf{b}\boldsymbol{\nu}^T\} = E\{\delta\bar{\mathbf{x}}\boldsymbol{\nu}^T\} = 0$. The preceding covariance may be expressed in the concise form

Table 4 Partial derivatives of scalars with respect to gain matrix

Matrix identity	Restrictions
$\frac{\partial f}{\partial K} = \begin{bmatrix} \partial f/\partial K_{11} & \cdots & \partial f/\partial K_{1m} \\ \vdots & \vdots & \vdots \\ \partial f/\partial K_{n1} & \cdots & \partial f/\partial K_{nm} \end{bmatrix}$	Scalar f $n \times m$ Matrix K
$\frac{\partial}{\partial K}(\text{tr}\{KL\}) = \frac{\partial}{\partial K}(\text{tr}\{L^T K^T\}) = L^T$	$n \times n$ Matrix KL
$\frac{\partial}{\partial K}(\text{tr}\{KNK^T\}) = 2KN$	$n \times n$ Symmetric matrix $N = N^T$

$\hat{P} = \bar{P} - KL - (KL)^T + KNK^T$, where

$$N = C\bar{P}C^T + MBM^T + R - C\bar{S}M^T - M\bar{S}^T C^T$$

and $L = C\bar{P} - M\bar{S}^T$. The optimal gain minimizes $\text{tr}\{\hat{P}\}$, such that

$$\frac{\partial}{\partial K}(\text{tr}\{\hat{P}\}) = \frac{\partial}{\partial K}(-\text{tr}\{KL\} - \text{tr}\{(KL)^T\} + \text{tr}\{KNK^T\}) = 2KN - 2L^T = 0$$

Partial derivatives of the trace terms are specified by matrix identities given in Table 4. It follows that optimal gain is specified by $K = L^T N^{-1}$.

References

[1] Okello, N., and Challa, S., "Joint Sensor Registration and Track-to-Track Fusion for Distributed Trackers," *IEEE Transactions on Aerospace and Electronic Systems*, Vol. 40, No. 3, July 2004, pp. 808–823. doi:10.1109/TAES.2004.1337456

[2] Lin, X., and Bar-Shalom, Y., "Multisensor Target Tracking Performance with Bias Compensation," *IEEE Transactions on Aerospace and Electronic Systems*, Vol. 42, No. 3, July 2006, pp. 1139–1149. doi:10.1109/TAES.2006.248212

[3] Friedland, B., "Treatment of Bias in Recursive Filtering," *IEEE Transactions on Automatic Control*, Vol. 14, No. 4, Aug. 1969, pp. 359–367. doi:10.1109/TAC.1969.1099223

[4] Friedland, B., "Notes on Separate-Bias Estimation," *IEEE Transactions on Automatic Control*, Vol. 23, No. 4, Aug. 1978, pp. 735–738. doi:10.1109/TAC.1978.1101789

[5] Alouani, A., Xia, P., Rice, T., and Blair, D., "On the Optimality of Two-Stage Estimation in the Presence of Random Bias," *IEEE Transactions on Automatic Control*, Vol. 38, No. 8, Aug. 1993, pp. 1279–1282. doi:10.1109/9.233168

[6] Lerro, D., and Bar-Shalom, Y., "Bias Compensation for Improved Recursive Bearings-Only Target State Estimation," *Proceedings of the American Control Conference*, Seattle, WA, IEEE Publ., Piscataway, NJ, June 1995, pp. 648–652.

[7] Myers, K., and Tapley, B., "Adaptive Sequential Estimation with Unknown Noise Statistics," *IEEE Transactions on Automatic Control*, Vol. 21, No. 4, Aug. 1976, pp. 520–523. doi:10.1109/TAC.1976.1101260

[8] Hough, M. E., "Recursive Bias Estimation and Orbit Determination," *Journal of Guidance, Control, and Dynamics*, Vol. 32, No. 2, March–April 2009, pp. 645–653. doi:10.2514/1.39955

[9] Smith, G., "Secondary Errors and Off-Design Conditions in Optimal Estimation of Space Vehicle Trajectories," NASA TN D-2129, Jan. 1964, pp. 20–26.

[10] Schmidt, S., "Application of State-Space Methods to Navigation Problems," *Advances in Control Systems*, Vol. 3, Academic Press, New York, 1966, pp. 293–340.

[11] Jazwinski, A., *Stochastic Processes and Filtering Theory*, Academic Press, New York, 1970, pp. 281–292.

[12] Tapley, B., *Statistical Orbit Determination*, Academic Press, New York, May 2004, pp. 387–438.

[13] Woodbury, D., and Junkins, J., "On the Consider Kalman Filter," AIAA Guidance, Navigation and Control Conference, Toronto, AIAA Paper 2010-7752, Aug. 2010.

[14] Bell, B., and Cathey, F., "The Iterated Kalman Filter Update as a Gauss–Newton Method," *IEEE Transactions on Automatic Control*, Vol. 38, No. 2, Feb. 1993, pp. 294–297. doi:10.1109/9.250476

[15] Fitzgerald, R., "Effects of Range-Doppler Coupling on Chirp Radar Tracking Accuracy," *IEEE Transactions on Aerospace and Electronic Systems*, Vol. AES-10, No. 4, July 1974, pp. 528–532. doi:10.1109/TAES.1974.307809

[16] Nickel, U., "Overview of Generalized Monopulse Estimation," *IEEE Aerospace and Electronic Systems Magazine*, Vol. 21, No. 6, June 2006, pp. 28–56. doi:10.1109/MAES.2006.1662006

[17] Barton, D., *Modern Radar System Analysis*, Artech House, Norwood, MA, 1988, pp. 302–310, 533–552.

[18] Bean, B., "Comparison of Observed Tropospheric Refraction with Values Computed from the Surface Refractivity," *IRE Transactions on Antennas and Propagation*, Vol. 9, No. 4, 1961, pp. 415–416. doi:10.1109/TAP.1961.1145019

[19] Altshuler, E., "Tropospheric Range-Error Corrections for the Global Positioning System," *IEEE Transactions on Antennas and Propagation*, Vol. 46, No. 5, May 1998, pp. 643–649. doi:10.1109/8.668906

[20] Hough, M. E., "Improved Performance of Recursive Tracking Filters Using Batch Initialization and Process Noise Adaptation," *Journal of Guidance, Control, and Dynamics*, Vol. 22, No. 5, Sept.–Oct. 1999, pp. 675–681. doi:10.2514/2.4457